Lattice Boltzmann Models with Mid-Range Interactions

Giacomo Falcucci[1], Gino Bella[2], Giancarlo Chiatti[1],
Sergio Chibbaro[2,3], Mauro Sbragaglia[4] and Sauro Succi[3,*]

[1] *Department of Mechanical and Industrial Engineering, University of "Roma Tre",
Via della Vasca Navale 79 00146 Rome, Italy.*
[2] *Department of Mechanical Engineering, University of "Tor Vergata", Viale
Politecnico, Rome, Italy.*
[3] *Istituto Applicazioni Calcolo, CNR, V.le del Policlinico 137, 00161, Rome, Italy.*
[4] *Faculty of Applied Sciences, Impact and Burgerscentrum, University of Twente,
P.O. Box 217, AE 7500 Enschede, The Netherlands.*

Abstract. An extension of the standard Shan-Chen model for non ideal-fluids, catering for mid-range, soft-core and hard-core repulsion, is investigated. It is shown that the inclusion of such mid-range interactions does not yield any visible enhancement of the density jump across the dense and light phases. Such an enhancement can however be obtained by tuning the exponents of the effective interaction. The results also indicate that the inclusion of soft-core repulsion can prevent the coalescence of neighborhood bubbles, thereby opening the possibility of tailoring the size of multi-droplet configurations, such as sprays and related phase-separating fluids.

1 Introduction

The Lattice-Boltzmann (LB) approach has proven to represent a powerful mesoscopic alternative to classical macroscopic methods for computational hydrodynamics [1,2]. The pseudopotential method put forward a decade ago by Shan-Chen to endow Lattice Boltzmann (LB) models with potential energy interactions, is one of the most successful outgrowth of basic LB theory [3, 4]. The Shan-Chen (SC) model is based on the idea of representing intermolecular interactions at the mesoscopic scale via a density-dependent

---

*Corresponding author. *Email addresses:* `falcucci@uniroma3.it` (G. Falcucci), `bella@uniroma2.it` (G. Bella), `chiatti@uniroma3.it` (G. Chiatti), `sergio.chibbaro@iac.cnr.it` (S. Chibbaro), `succi@iac.cnr.it` (S. Succi)

nearest-neighbor pseudopotential $\psi(\rho)$. Despite its highly simplified character, the SC model provides the essential ingredients of non-ideal (dense) fluid behavior, that is i) a non-ideal equation of state, ii) surface tension effects at phase interfaces. Because of its remarkable computational simplicity, the SC method is being used for a wide and growing body of complex flows applications, such as multiphase flows in chemical, manufacturing and geophysical problems.

In spite of its undeniable success, the SC method has made the object of intense criticism. In particular, i) lack of thermodynamic consistency, ii) spurious currents at interfaces and iii) surface tension tied-down to the equation of state. Problem i) refers to the fact that there is only one functional form, namely $\psi(\rho) \propto \rho$, securing compatibility between mechanical stability of the interface and equilibrium thermodynamics, i.e., Maxwell's area law in the Van der Walls loop of the non-ideal equation of state. However, recent studies [6] have clearly shown that the use of suitable pseudopotentials such that $\psi(\rho) \to \rho$ in the limit of zero density, makes this problem largely irrelevant to any practical purposes. Problem ii) is in general held responsible for setting a sharp limit on the density jumps across the dense/rarefied fluid interface to values around ten or less. This is a rather severe limitation for many practical applications, in which two-three orders of magnitude density jumps are often encountered (typically 1:1000 for air-water interfaces). Recent studies indicate that the density ratio can be drastically enhanced by resorting to different types of equations of state (EOS) other than the original one derived by Shan-Chen [7]. These new EOS are parametric variants of Van der Walls (VdW) equation of state, hence they include both hard-core short-range repulsion (absent in the SC model) and soft-core long-range attraction. Short-range repulsion is known to represent a potential danger for numerical stability, since it implies intense and localized interactions which may disrupt the numerical time-marching scheme. Hence, it is reasonable to wonder whether higher density ratios may be achieved by augmenting the original SC pseudopotentials with additional soft-core interactions and, more in general, which are the effects of such inclusion. This is precisely the route explored in this work.

2 Shan-Chen model with mid-range interactions

We consider the standard lattice Boltzmann (LB) equation with pseudopotentials

$$f_i(\vec{r}+\vec{c}_i,t+1) - f_i(\vec{r},t) = -\omega(f_i - f_i^{eq}) + F_i. \tag{2.1}$$

In the above, all symbols are standard, except for the pseudo-force F_i, as discussed below. We consider generalized pseudoforces of the following form

$$\vec{F}(\vec{r}) = \sum_{j=1}^{2} c_s^2 G_j \psi_j^{n(j)}(\rho(\vec{r})) \sum_{i=1}^{b_j} p_{ij} \vec{c}_{ij} \psi_j^{n(j)}(\rho(\vec{r}+\vec{c}_{ij})). \tag{2.2}$$

In the above, the index j labels the Seitz-Wigner cell (*belt* for simplicity) defined by the condition $|\vec{r'}-\vec{r}|^2 \le 2j^2$, whereas $\vec{c}_{ij}$ denotes the set of discrete speeds belonging to the j-th
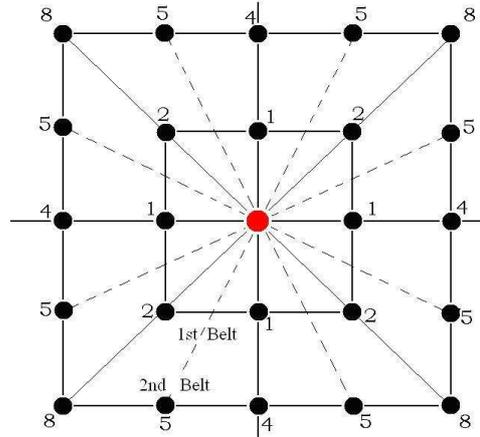
Figure 1: Two-belt lattice for force evaluation. Each node is labelled by the corresponding energy $|c_{ij}|^2$. Belt 1 contains eight speeds and two energy levels (1,2). Belt 2 contains sixteen speeds, distributed over three energy levels (4,5,8).

belt. The exponents $n(j)$ are chosen to be: $n(1)=1$ and $n(2)$ varying between 1 and $1/8$. Note that lattice units $\Delta x = \Delta t = 1$ have been assumed here. In this work we shall confine our attention to the 24-neighbors, 2-belt lattice depicted in Fig. 1.

As is well-known, the standard 1-belt, 8-speed lattice provides 4th-order isotropy, whereas the 2-belts, 24-speed lattice upgrades isotropy to 8-th order, provided the weights are properly chosen. A suitable choice is reported in Table 1.

To forestall any confusion, we wish emphasize that the 2-belt lattice is used *only* for the (pseudo)-force evaluation, whereas the standard lattice Boltzmann dynamics still takes place in the original D2Q9 lattice. This is also the reason why we keep a separate notation for the weights w_i used for the lattice Boltzmann populations and the weights p_{ij} used for the force evaluation.

In the case mostly used of $n(2)=1$, from equation (2.2) it is possible to find the equation of state of our system, which reads

$$p(\rho) = \rho c_s^2 + \frac{1}{2} G_1 C_1 c_s^2 \psi^2 + \frac{1}{2} G_2 C_2 c_s^2 \psi^2. \tag{2.3}$$

This can be recast as follows:

$$p(\rho) = \rho c_s^2 + \frac{1}{2} G_{eff} \psi^2 c_s^2, \tag{2.4}$$

where

$$G_{eff} = G_1 C_1 + G_2 C_2 \tag{2.5}$$

is an effective coupling and

$$c_s^2 = \sum_{i=0}^{8} w_i c_{i1,x}^2 = \frac{1}{3}, \quad C_1 = \sum_{i=1}^{8} p_{i1} c_{i1,x}^2 = \frac{737}{1000}, \quad C_2 = \sum_{i=1}^{16} p_{i2} c_{i2,x}^2 = \frac{33}{125}.$$

Table 1: Links and weights of the two-belt, 24-speed lattice [8].

E(8)	
$p_{i1} = p(1) = 4/21$,	$i = 1,4$
$p_{i1} = p(2) = 4/45$,	$i = 5,8$
$p_{i2} = p(4) = 1/60$,	$i = 1,4$
$p_{i2} = p(5) = 2/315$,	$i = 5,12$
$p_{i2} = p(8) = 1/5040$,	$i = 13,16$

At the level of the EOS, this is the same as the Shan-Chen model, just with a rescaled coupling. However, since repulsive forces act on the second belt of neighbors, they are distributed differently in space, and consequently their effect cannot be captured by a mere rescaling of the attractive interactions, possibly allowing density ratios to depend on G_1 and G_2 separately. From a qualitative point of view, this can be seen through a Taylor development of the coupling force. Indeed, the force given by Eq. (2.2) can be written in the continuum as

$$\vec{F}(\vec{r}) = G_{eff} c_s^2 \vec{\nabla} \psi + g(G_1, G_2) c_s^2 \vec{\nabla} \nabla^2 \psi + \mathcal{O}(\nabla^4), \qquad (2.6)$$

where

$$g(G_1, G_2) = G_1 \sum_{i=1}^{8} p_{i1} c_{ix}^4 + G_2 \sum_{i=1}^{16} p_{i2} c_{ix}^4.$$

This expression differs from the standard Shan-Chen model, since in the standard Shan-Chen both coefficients would be G_{eff}.

The two-parameter equation of state (2.3) offers an additional degree of freedom, G_2, as compared with the standard Shan-Chen. As recently shown [6], this degree of freedom can be used to tune the surface tension independently of the equation of state. In this work, the zone of attraction-repulsion (AR) and of repulsion-attraction (RA) potential have been considered. On one hand, the (RA) region corresponding to positive G_1 and negative G_2, may seem the most physical, since the hard-core repulsion could be associated with the first belt and the soft-core attraction with the successive belt.

On the other hand, the hard-core repulsion is felt only at distances of the order of molecular size, while the first neighbors in LB are well beyond these distances [5]. Thus, at least with present standard resolutions, the value of G_1 can be kept negative without losing physical sound. Moreover, mid-range repulsion is physically realized in (charged) colloid systems [9], although we shall not pursue this analogy any further in this paper. Next, we compute the critical value of the coupling strength G_{crit}, defined by the condition $\partial P / \partial \rho = 0$.

Treating G_2 as a free parameter, it is possible to find the value of G_1 such that the condition $\partial P / \partial \rho = 0$ is fulfilled, as a function of ψ, producing phase separation in accordance

with positive pressures from the equation of state. This condition reads

$$G_1 = -\frac{c_s^2}{(1-\psi)\psi C_1} - G_2 \frac{C_2}{C_1}. \tag{2.7}$$

We remind that in the standard Shan-Chen model, phase-separation is triggered by attractive interactions ($G_1 < 0$) between neighbors in the first belt. Attractive interactions enhance density gradients and consequently they promote a progressive steepening of the interface, eventually taking the system to a density collapse. In dense fluids and liquids such density collapse is prevented by short-range, hard-core repulsive forces, which stop the indefinite growth of density gradients, thereby stabilizing the fluid interface. In the Shan-Chen model, such a stabilizing effect is surrogated by imposing a saturation of the intermolecular attraction for densities above a reference value, ρ_0. This is a form of 'asymptotic freedom', for it implies that the interactions vanish at short-distance (high density). This mechanism is encoded into the functional form of the Shan-Chen potential

$$\psi(\rho) = \rho_0(1 - e^{-\rho/\rho_0}), \tag{2.8}$$

from which it is apparent that for densities above ρ_0, ψ tends to a constant, so that the corresponding force goes to zero. The inclusion of mid-range (second belt of neighbors) repulsion ($G_2 > 0$) provides a further stabilization mechanism, which, at variance with high-density saturation, acts preferentially on the low-density phase. This is easily seen by recognizing that, since $d\psi/d\rho = (1-\psi)$, the pseudo-potential force reads as

$$F = -\nabla\psi = -(1-\psi)\nabla\rho.$$

This expression shows that the pseudo-potential force is stronger on the low-density phase ($\psi \to 0$) than on the high-density one ($\psi \to 1$). In fact, the latter is basically left unaffected by the mid-range potential. The result is that the depletion of the low-density region caused by the destabilizing effect of the attractive forces is countered by the stabilizing action of the mid-range repulsive ones.

It is worth noting that the combination of short-range attraction and long-range repulsion, albeit potentially unstable (see the maximum of the AR potential in Fig. 2), is by no means devoid of physical meaning. Indeed, this type of interaction is widely studied in flows of (charged) colloids, coated with small polymer-coating molecules [9]. In such flows, the competition between short-range attraction due to the polymer coating, and long-range repulsion (typically a Yukawa potential) due to screened electrostatic interactions, gives rise to a very rich variety of structural behaviors, such as cluster formation, dynamically arrested gelation and many others. In this work, the motivation for long-range attraction is quite different, and namely to provide a stabilization mechanism of the interface growth. Yet, as it will be shown in the sequel, the competition between short range attraction and long-range repulsion may lead to interesting effects on the phase-separation properties of the LB fluid as well. It remains to be investigated whether
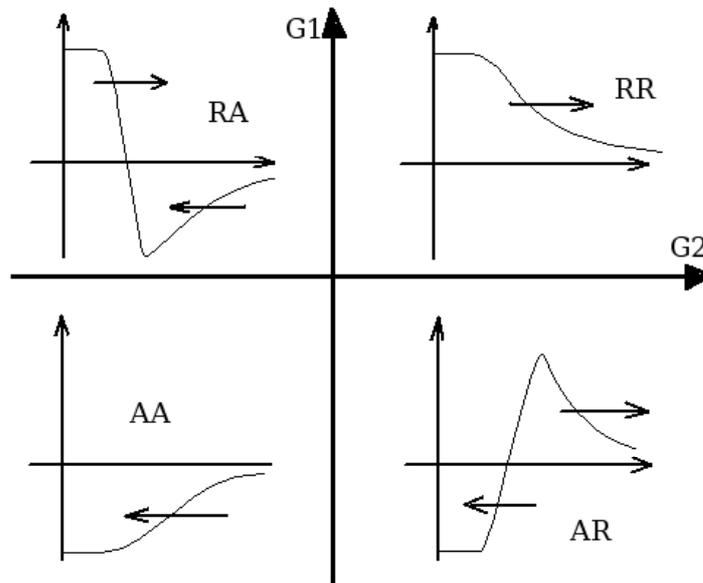
Figure 2: Sketch of the potentials associated with the four quadrants of (G_1, G_2) parameter space.

attractive forces can be made stronger than in the SC case, due to the presence of a repulsive interaction. This allows larger density contrasts, without incurring the numerical instabilities triggered by depletion of the low density phase (negative densities are the typical cause of Shan-Chen breakdown). As we shall see, the presence of such stabilization mechanism is indeed borne out by actual numerical simulations.

It is important to note that the choice of a G_{eff} too negative causes the pressure to become negative in Eq. (2.4). Although only pressure gradients come at play in general LB purposes, this range remains unphysical. In this concern, the standard Shan-Chen EOS starts to present negative pressures with an $\rho_l/\rho_g \sim 10$. The use of two parameters gives the opportunity, at least, to gauge the proportion between the attractive and repulsive contributions, while keeping the same G_{eff}.

The standard case of Shan-Chen is retrieved for $G_2 = 0$. The maximum given by the condition $\partial G_1/\partial \psi = 0$ defines the critical point, where the condition $\partial^2 P/\partial \rho^2 = 0$ is also fulfilled. Therefore, for this value of G_1 there is only one value of ρ for which the state is critical. For values of G_1 below this critical value, there are two values of ρ for which $\partial P/\partial \rho = 0$; that is the equation of state shows a maximum and a minimum of P in correspondence to these density values.

3   Results and discussion

We have performed a series of simulations of liquid droplet formation in a bulk gas phase. The simulations are performed on a 64×64 periodic box. The main parameters are $\rho_0 = 1$,
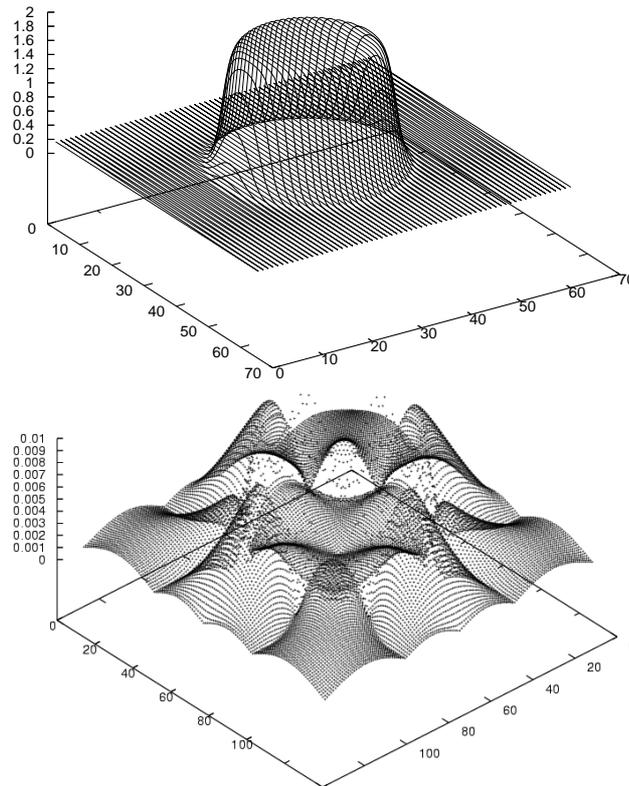
Figure 3: Droplet density distribution (top) and local Mach number (bottom) for the standard Shan-Chen model with $G_1 = -4.5$, corresponding to a density ratio of 5.6.

$\omega = 1$, the initial density $\rho_{init} = \ln 2$, with a localized random perturbation to excite the demixing transition.

First of all, we consider the standard Shan-Chen separation case, Fig. 3.

It is important to note that the density ratio achieved with the constraint of positive pressure is of order 10, with the value of the coefficient $G_1 = -4.9$. The surface tension corresponding to this case is $\sigma = 0.019$.

Next we analyze the results obtained adding the mid/range repulsion, thus the AR potential with linear interaction ($n(1)=1$). Choosing G_1 and G_2 such that the G_{eff} remains constant $G_{eff} = -4.5$, we have seen that the results are not influenced by the particular choice of the two parameters, concerning the macroscopic quantities. In Fig. 4, the results obtained with $G_1 = -7$ and $G_2 = 2.5$ are shown as the representative case. The density jump is not quantitatively different from that achieved by standard SC method. Also the spurious currents are in line with the standard approach. The surface tension has the value of $\sigma = 0.018$ and it is slightly lowered by means of the stabilizing mechanism provided by repulsion and described in the previous section.

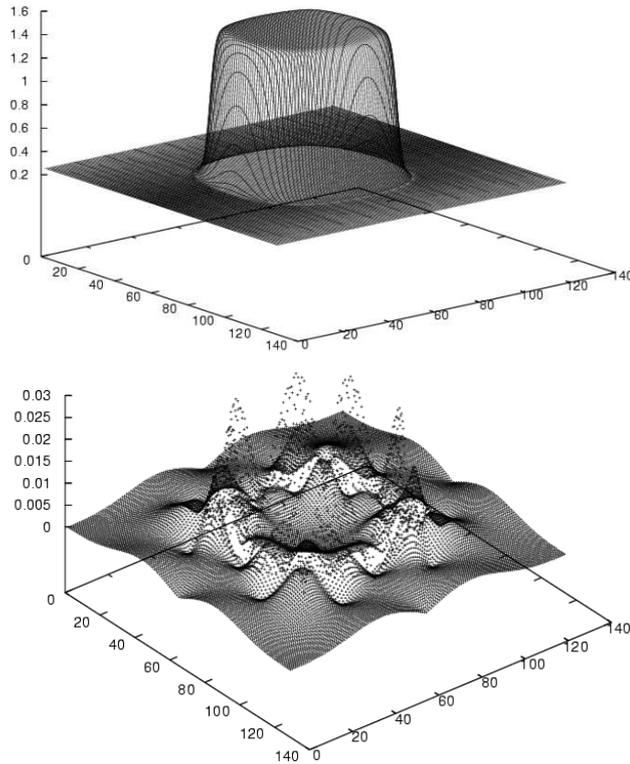In order to reach a higher density jump still with the constraint of a positive pressure,

Figure 4: Density profile (top) and local Mach number (bottom) with $G_1 = -7$ and $G_2 = 2.5$ corresponding to $G_{eff} = -4.5$ and $\rho_l/\rho_g = 5.6$.

it is necessary to choose a different form of the repulsive interaction. Notably, it can be shown that the optimal form is given by the choice $n(2) = 1/8$. In the case with density ratio $\rho_l/\rho_g \sim 40$, the spurious velocity M_s are everywhere lower than 0.3, where $M_s = u/c_s$ is the local mach number, see Fig. 5. Moreover, it is possible to see from Fig. 6 that the density ratio of $1:35$ is coherent with the equation of state, since pressure remains over zero. These results are obtained since the presence of a sub-linear repulsive force allows the existence of a broader pressure curve and, thus, the coexistence of two states with increased density ratio. Notwithstanding the significant improvement, it is worth reminding that the adopted form of interaction looks rather "exotic" and its applicability in actual experiments remains to be ascertained.

Next, we have studied the RA zone of the potential, considering different possibilities to reach the same G_{eff}. In Fig. 7, the density and the velocity obtained are shown. Even in this configuration, the macroscopic quantities (density jump, spurious currents) result in line with the standard ones. A little enhancement in the value of the surface tension is verified, $\sigma = 0.028$. Moreover, the same results are obtained whatever the values of G_1 and G_2, provided that the same G_{eff} is used.

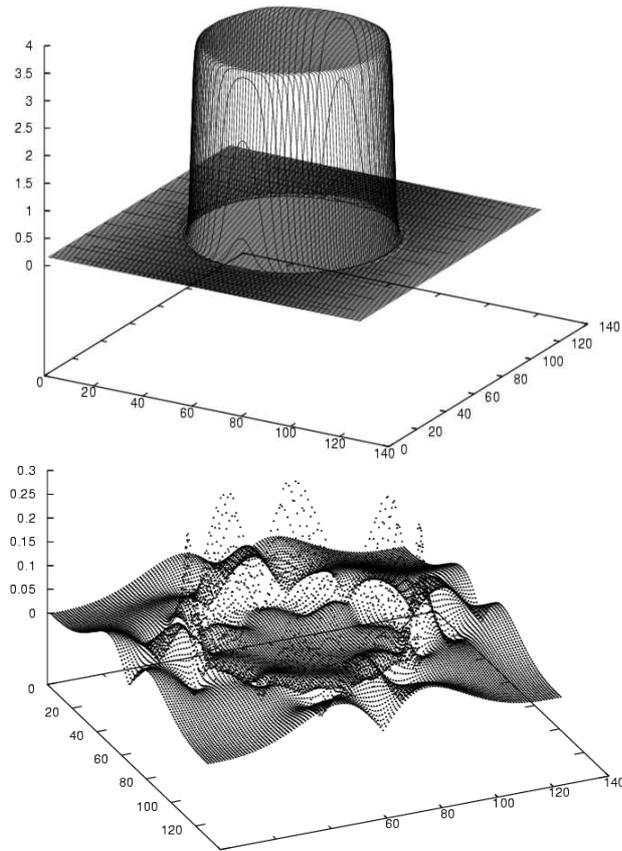Some remarks are in order. All the presented simulations, excepted the sub-linear

Figure 5: Droplet density (top) and local Mach number (bottom) distribution with the 2-belt model and $n(2)=1/8$: $G_1=-11.5$ and $G_2=9.0$. Density ratio is 1:35.
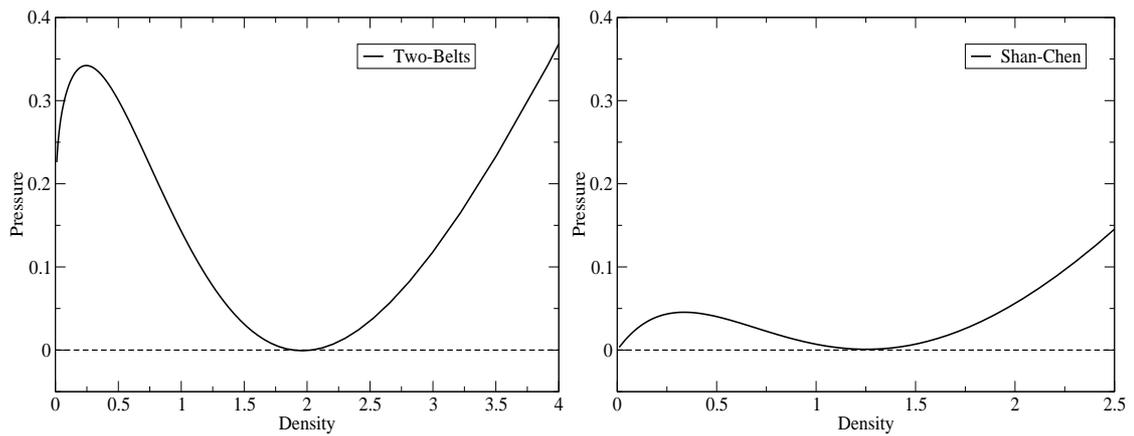

Figure 6: Equation of state corresponding to $G_1=-11.5$ and $G_2=9.0$ leading to $\rho_l/\rho_g=35$ (left). The corresponding SC curve, with $G_1=-4.9$ is shown for comparison (right).
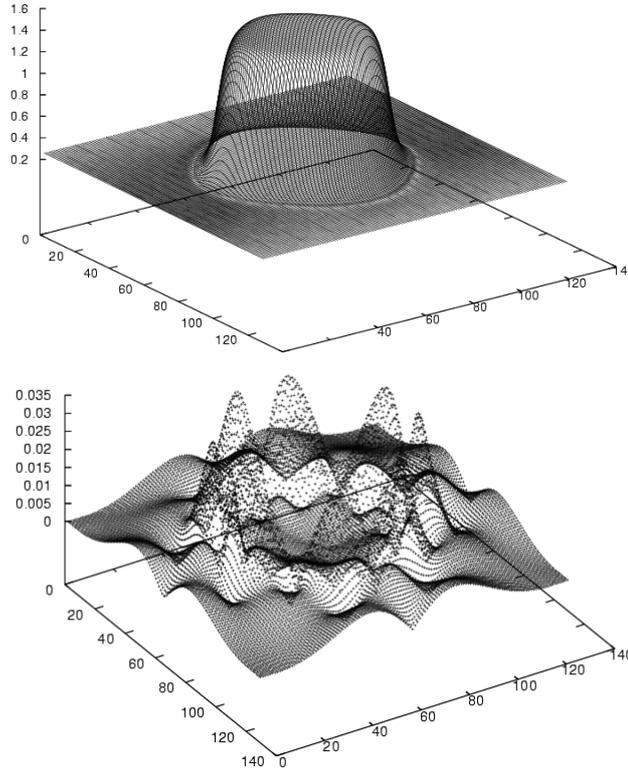
Figure 7: Density profile (top) and local Mach number (bottom) with $G_1 = 2.5$ and $G_2 = -24.02$ corresponding to $G_{eff} = -4.5$ and $\rho_l/\rho_g = 5.6$.

ones with $n(2) = 1/8$, have been carried out with the same value of G_{eff} and, thus, with the same profile of the pressure, see Eq. (2.4). We have seen that the corresponding macroscopic results are not sensitive to the different values of G_1 and G_2, being almost identical. Therefore, the only relevant factor for the control of density jump is the first-order term in the Taylor development of the force. The little changes in the surface tension values can be attributed to the effect of the higher-order terms.

To better understand the effects of G_2, it is possible to plot the forces due to G_1 and G_2 in the case of $n(2) = 1$:

$$\vec{F_1} = \frac{1}{2}G_1\psi(\vec{r})\sum_{i=1}^{b_1} w_i\psi(\vec{r}+\vec{c_i})\vec{c_i}, \tag{3.1}$$

$$\vec{F_2} = \frac{1}{2}G_2\psi(\vec{r})\sum_{i=1}^{b_2} w_i\psi(\vec{r}+\vec{c_i})\vec{c_i}. \tag{3.2}$$

Fig. 8 shows the trend of the x components of the force inside the calculation domain. The two members due to the two types of interaction are displayed and the presence of the density profile allows to locate their peaks. The density ratio in the two cases is
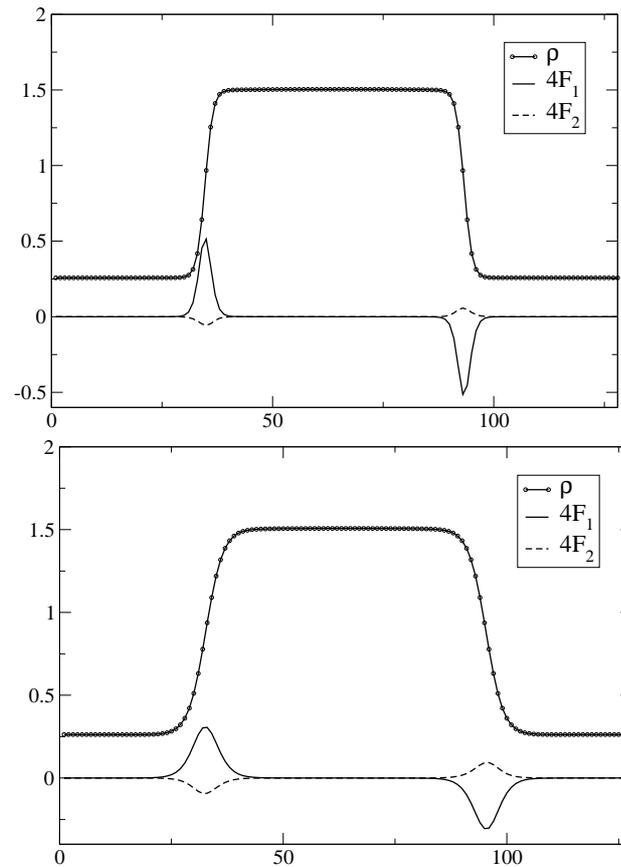
Figure 8: Density profile and total force x components inside the domain, with $G_1 = -7$ (top) and $G_1 = 2.5$ (bottom) corresponding to $G_{eff} = -4.5$ and $\rho_l/\rho_g = 5.6$.

the same, corresponding to $G_{eff} = -4.5$, but it is reached by means of an attractive or a repulsive G_1: the two pictures highlight the differences in the force field.

The second observation, related to the previous one, is that F_{2x} is shifted away from the interface as compared to F_{1x}. This is in line with the expectation that a different spatial distribution implies that the effect of F_2 does not reduce to a mere rescaling of the attractive interactions, as it would indeed be the case had we placed repulsive interactions on the first belt, like the attractive ones. The attractive force has its maximum in the center of the interface, for the effect of density variation. In general, the net effect of the short-range attractive force is to push particles from the interface to the liquid phase (that is, from gas to liquid), improving the phase-transition and keeping the surface-tension. On the other hand, the repulsive force has its maximum at the end of the interface on the liquid side and its global effect is to counter the depletion of gas particles. Moreover, being non-local, the repulsive force is also responsible for the effect of accumulation of liquid particles at the interface. Indeed, while the short-range attractive force is zero far
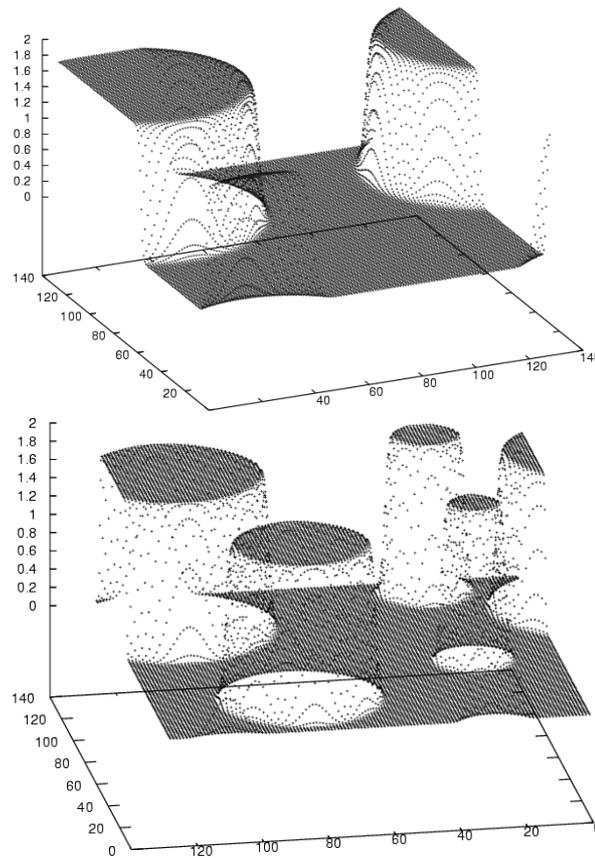
Figure 9: Density profiles in a randomly perturbated field after 10000 time steps: the standard Shan-Chen case coalesces (top) while the complete E(8) lattice (bottom) presents different droplets; $G_{sc} = -4.9$ and $G_1 = -11$, $G_2 = 6.1$ corresponding to $G_{eff} = -4.9$ and $\rho_l / \rho_g = 10.6$.

from the interface, the mid-range repulsive force persists one site farther from the interface because of the non-locality. Thus, in this region the repulsive force prevails. This means that there is a (tiny) region where the net non-ideal force is repulsive, an effect which goes beyond the equation of state where the net non-ideal contribution is always attractive. However, this effect is so small that it is not perceived at macroscopic level.

At the same time, this non-local effect can play an important role in other problems. In particular, with the repulsive force acting on the two belts and the attractive one only in the first, it is possible to see an 'anti-coalescence' effect of the repulsive interaction, as shown in Fig. 9.

Although this phenomenon is still under investigation, the possibility of using small mid-range repulsive force to simulate some "impurity effects" that change drastically the evolution of the system after the phase transition, looks quite intriguing.

Finally, the non-equilibrium behavior of the present model is tested against the stan-
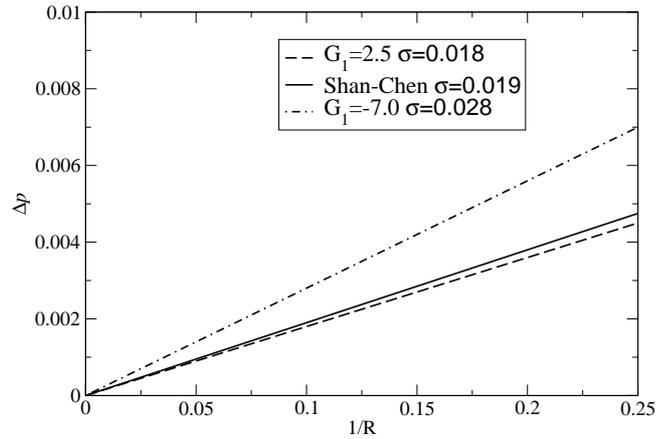
Figure 10: Laplace test: SC with $G_1 = -4.5$, and $\rho_l/\rho_g = 5.6$; 2-belts with $G_1 = -7$, $G_2 = 2.5$ and 2-belts with $G_1 = 2.5$, $G_2 = -24.02$, corresponding to the same ρ_l/ρ_g as the standard Shan-Chen case.

dard Laplace's law

$$P_l - P_g = \frac{\sigma}{R},$$

where σ is the surface tension and R the droplet radius. As shown in Fig. 10, Laplace's law holds to a good accuracy. It is also noted that by making G_1 more negative, with a fixed G_{eff}, the value of the surface tension is of the same order magnitude as with standard SC scheme. In practice, adding a repulsive force with $G_2 > 0$ results in a more stable method and allows to keep $|G_1| \gg 1$. Nevertheless, it also tends to weaken the surface tension, by continuously pushing particles towards the interface, so that the combined effect of the two is rather negligible.

4 Conclusions

In conclusion, we have analyzed the effects of the inclusion of a mid-range potential on top of the standard Shan-Chen pseudo-potential model. The present simulations provide clear indications that this mechanism permits a significant enhancement of the short-range attractive force with a strong stabilizing effect, yet without important changes in the macroscopic behavior. Nevertheless, the presence of a mid-range repulsive force changes the surface tension and seems to be able to mimic the presence of impurities which prevent the coalescence of the droplets. Therefore, the mid-range interactions may have a significant effect on the microscopic behavior of the phase-separating system.

Future work including further neighbors and multiple species [10] is currently in progress.

Finally, we wish to emphasize that in this work, we have chosen to work within the constraint of positive fluid pressure, $p \geq 0$: that is repulsive interactions (ideal plus mid-range non-ideal) always prevail over (non-ideal) attractive ones. However, it is empir-

ically observed that both standard SC and the present model keep providing sensible results in the unphysical $p < 0$ region, actually with enhanced density jumps. This raises the question of whether recent studies reporting density ratios as high as 1:1000 are indeed compliant with the $p \geq 0$ constraint. Another intriguing question, to be left for future studies, is whether it makes sense to operate LB in the unphysical region $p < 0$: the possibility of negative pressure has been speculated for exotic states of matter, characterized by dominant attractive interactions, such as Bose-Einstein condensates, or quintessence and dark matter in cosmological flows [11].

References

[1] S. Succi, The Lattice Boltzmann Equation for Fluid Dynamics and Beyond, Oxford Science Publications, 2001.
[2] R. Benzi, S. Succi and M. Vergassola, The lattice Boltzmann equation: Theory and applications, Phys. Rep., 222 (1992), 145-197.
[3] X. Shan and H. Chen, Lattice Boltzmann model for simulating flows with multiple phases and components, Phys. Rev. E, 47 (1993), 1815-1819.
[4] X. Shan and H. Chen, Simulation of nonideal gases and liquid-gas phase transitions by the lattice Boltzmann equation, Phys. Rev. E, 49 (1994), 2941-2948.
[5] R. Benzi, Private communication.
[6] M. Sbragaglia, R. Benzi, L. Biferale, S. Succi, K. Sugiyama and F. Toschi, Generalized lattice Boltzmann method with multi-range pseudo-potential, Phys. Rev. E, 75 (2007), 026702.
[7] P. Yuan and L. Schaefer, Equations of state in a lattice Boltzmann model, Phys. Fluids, 18 (2006), 042101.
[8] X. Shan, Analysis of the spurious current near the interface in a class of multiphase lattice Boltzmann models, Phys. Rev. E, 73 (2006), 047701.
[9] A. I. Campbell, V. J. Anderson, J. S. Van Duijneveldt and P. Barlett, Dynamical arrest in attractive colloids: The effect of long-range repulsion, Phys. Rev. Lett., 94 (2005), 208302.
[10] S. V. Lishchuk, A. M. Care and I. Halliday, Lattice Boltzmann algorithm for surface tension with greatly reduced microcurrents, Phys. Rev. E, 67 (2003), 036701.
[11] J. Khoury and A. Weltman, Chameleon fields: Awaiting surprises for tests of gravity in space, Phys. Rev. Lett., 93 (2004), 171104.